

# Galactic diffuse gamma rays — a recalculation based on the new results of cosmic electron spectrum

Juan Zhang<sup>1</sup>, Qiang Yuan<sup>1</sup>, Xiao-Jun Bi<sup>2,1</sup>

<sup>1</sup> *Key Laboratory of Particle Astrophysics, Institute of High Energy Physics, Chinese Academy of Sciences, Beijing 100049, P. R. China*

<sup>2</sup> *Center for High Energy Physics, Peking University, Beijing 100871, China*

## Abstract

In this work we revisit the all-sky Galactic diffuse  $\gamma$ -ray emission based on the “conventional” cosmic ray model. The major revision to the “conventional” cosmic ray model is to accommodate the new results of cosmic electrons/positrons from PAMELA, ATIC, PPB-BETS, H.E.S.S. and Fermi-LAT, which show excesses of electrons or positrons compared with the expected background. However, as the origins of the excesses are not clear, we consider different scenarios to account for the excesses: the astrophysical sources, such as the Galactic pulsars, or exotic sources, such as dark matter annihilation or decay. We find the EGRET data can set strong constraints on the dark matter annihilation scenario. While there are few constraints on the decaying dark matter and pulsar scenarios. Furthermore, we find some distinctive features at the diffuse  $\gamma$ -ray spectra for the dark matter scenarios. We expect that measurements at Fermi-LAT up to  $\sim 300$  GeV may have the potential to distinguish, or at least set strong constraints on, the dark matter scenarios.

## I. INTRODUCTION

The diffuse Galactic  $\gamma$ -ray is an important issue to astrophysics, since it provides a direct measurement of cosmic rays (CRs) at distant locations. It provides a crucial diagnostic of the transportation process of CRs in the interstellar space. Further it forms the foreground of the extragalactic diffuse  $\gamma$ -ray emission. The diffuse Galactic  $\gamma$ -rays may also provide information of exotic sources, such as the dark matter (DM) annihilation or decay.

The diffuse Galactic  $\gamma$ -rays are generally produced through, 1) the decay of  $\pi^0$  produced from interactions between CR nuclei and interstellar medium (ISM), 2) inverse Compton (IC) scattering of CR electrons/positrons with interstellar radiation field (ISRF), and 3) bremsstrahlung radiation of the electrons/positrons when interacting with ISM. Since the  $\gamma$ -ray is not deflected by the magnetic field when propagating through the interstellar space, it can trace the distribution of CR sources, ISM, ISRF and so on. The  $\gamma$ -rays are regarded as a very powerful probe to study the origin, propagation and interaction of CRs.

The propagation of CRs in the Galaxy is usually described by a diffusive process that charged particles are scattered by the random Galactic magnetic fields. Interactions, energy losses or regain are also considered in the propagation processes. A comprehensive description of the cosmic rays propagation and diffusive  $\gamma$ -ray emission via interaction between CRs and the ISM are developed as a computer package, the GALPROP [1, 2]. The GALPROP tries to determine the propagation parameters by fitting all the CR data. Especially it gives proton and electron spectra at the position of solar system consistent with that observed by the local experiments. This model is called the “conventional” CR propagation model, which is very successful to fit all the CR data, as well as the diffuse  $\gamma$ -ray data by EGRET, except the well known “GeV excess” problem [3]. The “GeV excess” problem has stimulated a lot of interests. The explanations range from the instrumental effect [4], changes of CR flux spectra or normalizations [5, 6, 7] and contribution of DM annihilation [8, 9, 10, 11].

Recently the observations on the CR positron fraction by PAMELA experiment [12] and the total electron and positron spectra by ATIC [13], PPB-BETS [14], H.E.S.S. [15, 16] and Fermi-LAT [17] all show interesting excesses when comparing with the conventional astrophysical background, that adopted by GALPROP. Unfortunately the origin of the excesses are not clear yet. Many possible origins have been proposed to explain the results, including astrophysical scenarios (e.g., [18, 19, 20, 21, 22]), and the models with exotic

new physics like dark matter (DM, e.g. [23, 24, 25, 26]). Since the electrons have important contribution to the diffuse  $\gamma$ -ray emission especially at high Galactic latitudes, it is necessary to revisit the problem of diffuse Galactic  $\gamma$ -ray emission after incorporating the new electron spectra. On the other hand, the diffuse  $\gamma$ -ray spectra can also be taken as a useful tool to probe the origin of the electron/positron excesses. Actually there have been some works in the literature shown that the associated  $\gamma$ -rays can be used to probe the origins of the electron/positron excesses [27, 28, 29, 30].

The Fermi-LAT collaboration also reported some preliminary results about the diffuse  $\gamma$ -ray emission at mid-latitude [31] and the inner Galaxy<sup>1</sup>. Interestingly, no clear excess at GeV band is observed by Fermi-LAT. It was illustrated that the excess electrons/positrons had little effect on the diffuse  $\gamma$ -ray spectra compared with the current observational results at mid-latitude [32, 33]. However, the preliminary results of Fermi-LAT about the inner Galaxy were shown to be consistent with a DM annihilation scenario [34]. Since the Fermi-LAT satellite is expected to give the all-sky diffuse  $\gamma$ -ray spectra up to  $\sim 300$  GeV in the near future, it is necessary to study the  $\gamma$ -ray emission in other sky regions taking into account the contribution from the extra electrons/positrons.

In this work, we investigate the all-sky diffuse  $\gamma$ -rays for the most popular three kinds of models which can explain the electron/positron excesses: Galactic pulsars, DM annihilation and DM decay. These models represent three typical types of spatial distributions of the electron/positron sources, i.e., disc-like distributions, highly concentrated spherical halo (DM annihilation) and less concentrated spherical halo (DM decay) respectively. For other models the conclusions are expected to be similar with one of those. The DM substructures from the recent most high resolution simulation [35] are included in our study.

In the following, we will first describe the (background) diffuse  $\gamma$ -ray emission based on the CR data before the newest experiments in Sec. II, and then simply introduce the three kinds of models to recover the CR electron/positron excesses in Sec. III. The all-sky diffuse  $\gamma$ -ray spectra in the new frame with extra electron/positron sources are presented in Sec. IV. Finally we give the conclusion and discussion in Sec. V.

---

<sup>1</sup> Talk at TeV Particle Astrophysics 2009 (TeVPA09), see <http://www-conf.slac.stanford.edu/tevpa09>

## II. CONVENTIONAL DIFFUSE $\gamma$ -RAY EMISSION

The Galactic diffuse  $\gamma$ -rays are produced through CRs interaction with the ISM. In this work we adopt GALPROP to calculate the propagation of CRs and the production of  $\gamma$ -rays. The propagation parameters are adjusted to reproduce all kinds of the low energy CR data such as B/C,  $^{10}\text{Be}/^9\text{Be}$ , the local proton and electron spectra [26]. The half height of the propagation halo is  $z_h = 4$  kpc, which is the same as that taken by Strong et al. in their conventional and optimized models [7]. The diffusion coefficient  $D_{xx} = \beta D_0(\rho/\rho_0)^\delta$  with  $D_0 = 3.0 \times 10^{28} \text{ cm}^2 \text{ s}^{-1}$ ,  $\delta = 0.50$  for rigidity  $\rho > 4$  GV and  $\delta = 0$  for  $\rho < 4$  GV. A convection+diffusion model is adopted with the convection velocity as a linear function of coordinate  $z$  with  $V_c(z = 0) = 0$  and  $dV_c/dz = 4 \text{ km s}^{-1} \text{ kpc}^{-1}$ . The injection spectra of nuclei share the same power law form in rigidity with power index 2.36 and nuclei up to  $Z = 28$  with all relevant isotopes included. The injection spectra of primary electrons are 1.50/2.52 when the rigidity is below/above 4 GV. Note that in order to be better consistent with the observational data after including the extra component (see below and also Ref. [28]), we adopt a slightly lower normalization ( $\sim 0.9$ ) of the primary electrons compared with the conventional model given in Ref. [7]. The reacceleration is not included. Actually for the reacceleration model the diffuse  $\gamma$ -ray spectra are almost the same as the convection model when all the CR data are fitted well. In Fig. 1 we show the model predictions of B/C ratio, the  $^{10}\text{Be}/^9\text{Be}$  ratio, and the local proton and electron spectra compared with data.

To describe the Galactic diffuse  $\gamma$ -ray emission at all directions we follow Strong et al. [7] to divide the whole sky into six regions: region A corresponds to the “inner radian”, region B is the Galactic plane excluding the inner radian, region C is the “outer Galaxy”, regions D and E cover higher latitudes at all longitudes, and region F describes the “Galactic poles”. The calculated diffuse  $\gamma$ -ray spectra in the six different sky regions are given in Fig. 2. The diffuse  $\gamma$ -ray background includes contributions from  $\pi^0$  decays produced by nuclei collisions, IC scattering off the interstellar radiation field (ISRF), bremsstrahlung by electrons, and the isotropic extragalactic  $\gamma$ -ray background (EGRB). The EGRB from 30 MeV to 20 GeV is adopted from Ref. [36]. As for the extrapolation to higher energies of the EGRB we use a fitted power law form  $2.72 \times 10^{-3} E^{-2.16} \text{ cm}^{-2} \text{ s}^{-1} \text{ sr}^{-1} \text{ MeV}^{-1}$  according to the one given in Ref. [36]. For the regions A, B, C and D, i.e. the Galactic plane and the intermediate latitude regions, the  $\pi^0$  decay contribution is dominant. At high latitude regions E and F

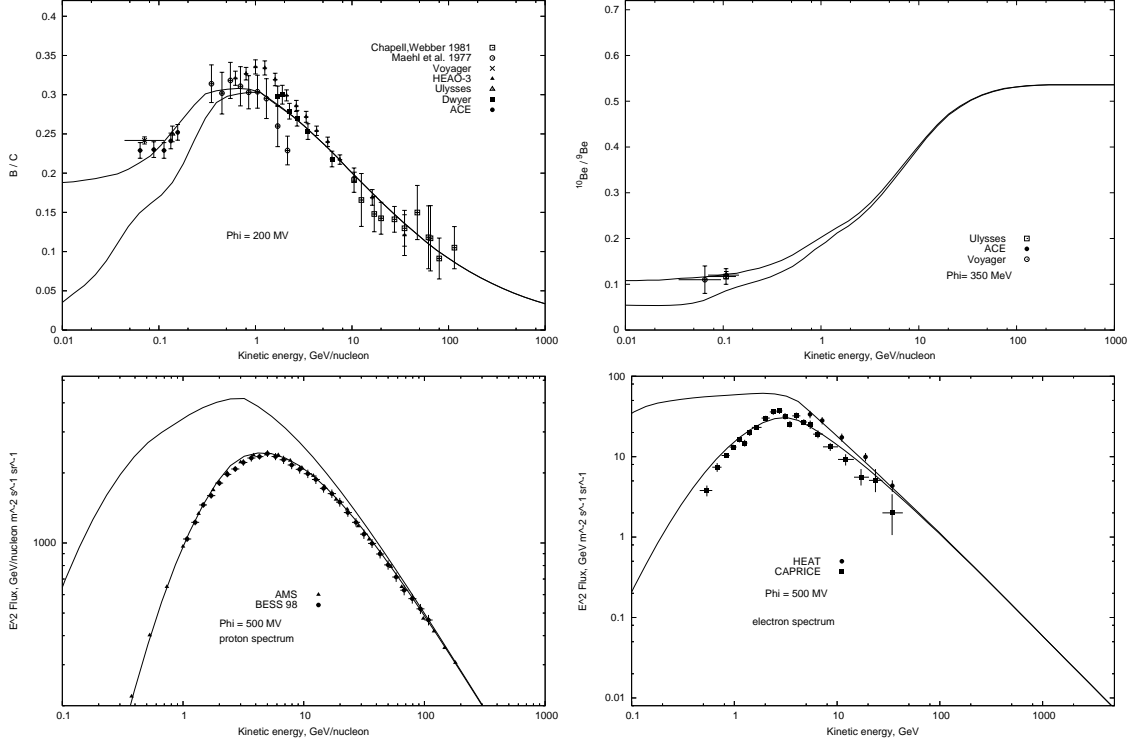


FIG. 1: CR results in our conventional model. Lower and upper curves for B/C and  $^{10}\text{Be}/^9\text{Be}$  ratios correspond to the local interstellar (LIS) result and the solar modulated one respectively. On the contrary, for proton and electron spectra the lower curves are the modulated ones and the upper curves are for LIS. B/C data are from Chapell-Webber [59], Maehl et al. [60], Voyager [61], HEAO-3 [62], Ulysses [63], Dwyer [64], ACE [65];  $^{10}\text{Be}/^9\text{Be}$  data from Ulysses [66], ACE [67] and Voyager [61]; proton data from AMS [69] and BESS98 [68]; electron data from HEAT [71] and CAPRICE [70].

the EGRB becomes more important.

We notice that the diffuse  $\gamma$ -ray emission of this conventional model at all directions are well consistent with the EGRET data except the “GeV excess”. In the region D, we also plot the preliminary Fermi-LAT data, which are well consistent with the model prediction. Therefore we expect the conventional CR model, that the local proton and electron spectra are consistent with data, will reproduce the Galactic diffuse  $\gamma$ -rays well.

However, in Fig. 1 we adopt the electron spectrum to fit the data before PAMELA, ATIC and Fermi-LAT results. In the next section we will show that the new experimental results of the electron spectrum show clear excess above this background. The diffuse  $\gamma$ -ray

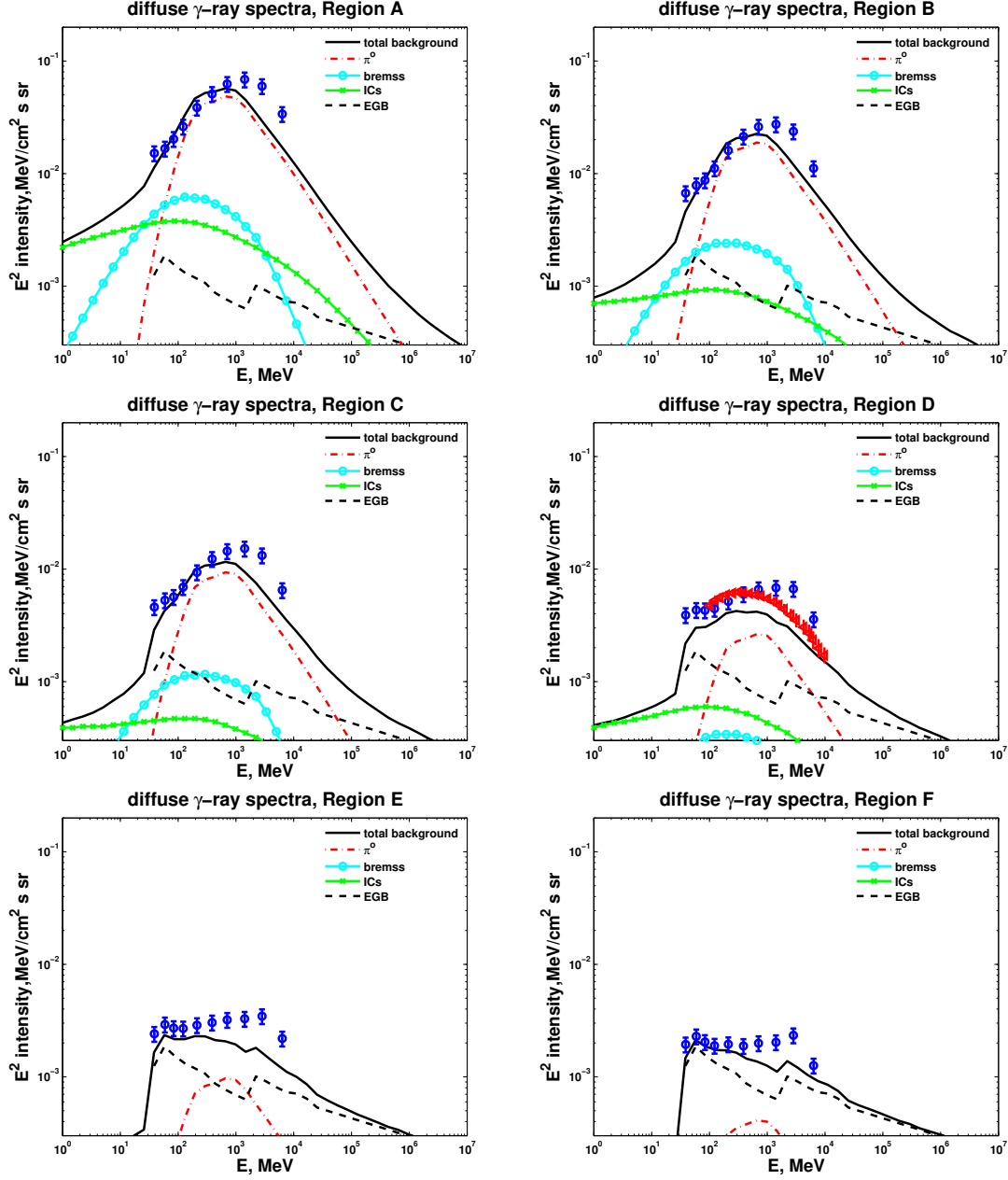


FIG. 2: Spectra of diffuse  $\gamma$ -rays for different sky regions (top row, regions A, B, middle C, D, bottom E, F). The model components are  $\pi^0$  decay, inverse Compton, bremsstrahlung, and EGRB.

emission has to be revisited according to these new data.

### III. SCENARIOS TO ACCOUNT FOR THE ELECTRON/POSITRON EXCESSES

#### A. Background

We usually refer to the electron flux in the conventional CR model as the background. As we have shown at last section the background can reproduce the EGRET (except “GeV excesses”) and Fermi-LAT diffuse  $\gamma$ -ray spectra very well. However, the recent experimental results of the electron spectrum from ATIC [13], Fermi-LAT [17] and H.E.S.S. [15, 16] all show clear excesses above the background in the conventional model. Note that, there are indeed large uncertainties on both the positron and electron spectra calculation. As shown in Refs. [37] and [38] one can fit either the positron fraction data or the total electron + positron data through the adjust of the background contribution. However, it is shown to be very difficult to explain the positron fraction and electron + positron spectra data simultaneously just using the background contribution [38].

A direct way to solve the anomalies is to add new primary sources which can generate electrons and positrons with equal amount. It is found by adopting proper spectrum of the primary electrons and positrons and the conventional electron background the ATIC or Fermi spectrum and the PAMELA positron ratio can be explained simultaneously (e.g., [28] and many others).

One should also note that the  $\bar{p}/p$  ratio predicted by the conventional model is well consistent with the PAMELA data [39], which means the primary electrons/positrons sources should be leptonic.

#### B. Galactic pulsars

The electron/positron excesses observed at the CR experiments may come from some nearby astrophysical sources. A possible candidate of such sources is the Galactic pulsars. Pulsars and their nebulae are well known cosmic particle accelerators. Although the quantitative details of the acceleration processes are still open for study, early radio observations have established them as important high energy cosmic electron and positron sources (e.g., [40]). X-ray and  $\gamma$ -ray observations show that some of the accelerated particles can reach an energy of a few tens of TeV, and there are indications that the particle distribution cuts off in the TeV energy range (e.g., [41, 42, 43]). These particles produce emission over a

broadband frequency range in the source region, which has been observed and studied extensively (e.g., [44]). Some of these particles will escape into the ISM becoming high energy cosmic electrons and positrons. It is shown that one or several nearby pulsars will be able to contribute enough positrons to reproduce the PAMELA data [18, 19] as well as ATIC data [20].

In our calculation the source term for Galactic pulsars is parametrized as

$$q(R, z, E)|_P = K f(R, z) \left. \frac{dN}{dE} \right|_P, \quad (1)$$

where  $K$  is the normalization factor representing the total luminosity of pulsars,  $f(R, z)$  is the pulsar spatial distribution with  $R$  the Galactocentric radius and  $z$  the distance away from the Galactic Plane, and  $\left. \frac{dN}{dE} \right|_P$  is the average electron/positron energy spectrum generated from pulsars. The spatial distribution of pulsars can be parametrized as

$$f(R, z) \propto \left( \frac{R}{R_\odot} \right)^a \exp \left[ -\frac{b(R - R_\odot)}{R_\odot} \right] \exp \left( -\frac{|z|}{z_s} \right), \quad (2)$$

in which the parameters are adopted as  $a = 1.0$ ,  $b = 1.8$  [45]. Different from the spherically symmetric form of DM distribution, pulsars are mainly concentrated at the Galactic Plane with  $z_s \sim 0.2$  kpc.

The primary electron/positron spectrum injected by pulsars is generally assumed to be a power law form with an exponential cutoff at high energies

$$\left. \frac{dN}{dE} \right|_P = E^{-\alpha} \exp \left( -\frac{E}{E_{\text{cut}}} \right). \quad (3)$$

We will discuss the parameters in the following.

### C. Dark matter models

Observations show that the Galaxy is dominated by dark matter. Many dark matter candidates have been proposed in the literature [46, 47]. The most attractive DM candidate is the weakly interacting massive particles (WIMP), which exist naturally in these models beyond the standard model, such as neutralinos in the supersymmetric models or the KK particles in the universal extra dimension models [46, 47]. These DM particles may decay at a very slow rate or annihilate into standard model particles, such as  $\gamma$ -rays, positrons/electrons and so on. Therefore the positron and electron excesses at the CR experiments have been widely considered as possible signals from DM decay or annihilation [23, 24, 25, 26].

Similar to the case of Galactic pulsars we incorporate these electron/positron sources from DM annihilation or decay in the GALPROP package so that we can calculate the fluxes on the Earth. We use the same propagation model as described above to calculate the contribution to electrons and positrons from the DM sources. The source function for DM annihilation and decay can be written as

$$q(\mathbf{r}, E)|_A = \frac{\langle\sigma v\rangle}{2m_\chi^2} \frac{dN}{dE} \Big|_A \rho^2(\mathbf{r}), \quad (4)$$

$$q(\mathbf{r}, E)|_D = \frac{1}{m_\chi\tau} \frac{dN}{dE} \Big|_D \rho(\mathbf{r}), \quad (5)$$

where  $m_\chi$  is the mass of DM particle,  $\langle\sigma v\rangle$  (or  $\tau$ ) is the annihilation cross section (or life-time of DM particles),  $\frac{dN}{dE}$  is the electron/positron yield spectrum for specified channel per annihilation or decay. In this work we assume the DM annihilation or decay directly into leptons, i.e.,  $\chi\chi \rightarrow e^+e^-, \mu^+\mu^-, \tau^+\tau^-$ . PYTHIA package [48] is used to simulate the radiative and decaying processes of the final state particles. Finally  $\rho(\mathbf{r})$  is the density profile of the Milky Way halo, for which we take an Einasto form [49]

$$\rho(r) = \rho_0 \exp \left[ -\frac{2}{\alpha} \left( \frac{r^\alpha - R_\odot^\alpha}{r_{-2}^\alpha} \right) \right], \quad (6)$$

with  $\alpha = 0.2$ ,  $r_{-2} = 25$  kpc and the local DM density  $\rho_\odot = 0.3 \text{ GeV cm}^{-3}$  at  $r = R_\odot \equiv 8.5$  kpc. The total mass of the halo inside the virial radius  $r_{\text{vir}} \approx 220$  kpc, within which the mean density is 200 times the critical density, is measured to be  $\sim 1.25 \times 10^{12} M_\odot$ . This profile was also able to fit the WMAP haze data [50] assuming DM annihilation to produce electrons/positrons [28].

We also include the DM substructures in our calculation according to the newest *Aquarius* N-body simulation of DM structure formation [35]. The annihilation luminosity, defined as  $L \propto \int \rho^2 dV$ , of the substructures can be scaled with respect to the smooth halo as [35, 51]

$$L_{\text{sub}}(< r) = 0.8 L_{\text{sm}} \left( \frac{M_{\text{min}}}{10^5 M_\odot} \right)^{-0.226} \left( \frac{r}{r_{\text{vir}}} \right)^{0.8(r/r_{\text{vir}})^{-0.315}}, \quad (7)$$

where  $L_{\text{sm}}$  is the luminosity of the smooth halo,  $M_{\text{min}}$  is the minimum subhalo mass corresponding to the free streaming of DM particles. We will adopt  $M_{\text{min}} \approx 10^{-6} M_\odot$ , which is the canonical value for cold DM particles [52, 53]. The mass fraction of the subhalos is estimated to be  $\sim 18\%$  in the *Aquarius* simulation [54]. Thus for the annihilation DM case, we rescale Eq. (6) with a factor of 0.82 when calculating the contribution from the smooth halo.

For the decaying DM case, there will be almost no effect for substructures. Therefore we regard the halo as a whole with density distribution following Eq. (6).

In Fig. 3 we show how the PAMELA and ATIC/Fermi results are explained by adding different primary sources, the pulsars, DM annihilation or decay. In this illustration plot we assume the mass of DM particle is 1 TeV for annihilation case (or 2 TeV for decaying case) and the final states are  $e^+e^-$ ,  $\mu^+\mu^-$  and  $\tau^+\tau^-$  with equal branching ratios. For pulsar model we adopt  $\alpha \approx 1.0$  and  $E_{\text{cut}} \approx 600$  GeV in Eq. (3). These model parameters are adopted to fit to PAMELA + ATIC data. However, slightly adjusting the parameters we can also give good fits to the Fermi-LAT and H.E.S.S. electrons, which are not shown here.

In summary, by taking proper parameters for these different primary sources the local measures of the electron/positron spectrum can be well explained. However, as we noticed that the spatial distribution of these scenarios are very different. Due the global nature of the diffuse  $\gamma$ -rays, we expect the diffuse  $\gamma$ -ray spectra should be different when taking different primary sources.

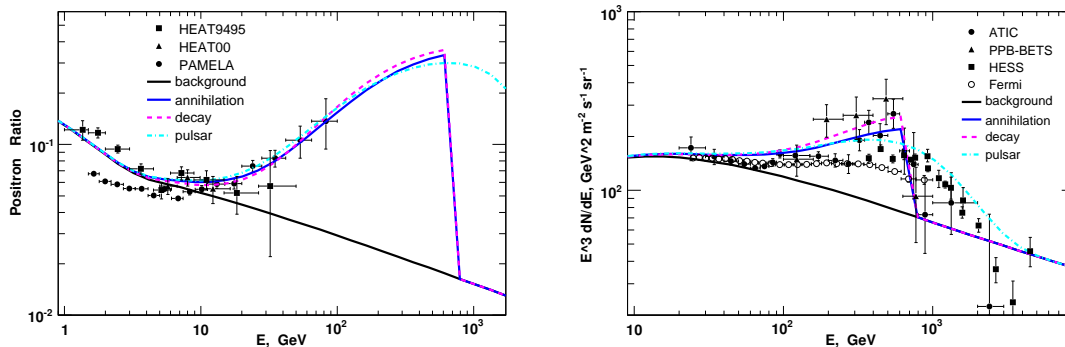


FIG. 3: *Left:* The positron fractions predicted by the three scenarios after solar modulation, compared with HEAT [72, 73] and PAMELA [12] data. *Right:* The total electron + positron fluxes of the three scenarios, compared with observations of ATIC [13], PPB-BETS [14], H.E.S.S. [15, 16] and Fermi-LAT [17].

#### IV. REVISED DIFFUSE $\gamma$ -RAY EMISSION

In this section we will present the results of the Galactic diffuse  $\gamma$ -ray spectra at all sky directions. In addition to the conventional background of the diffuse  $\gamma$ -rays the primary

electron/positron sources to account for the new CR data are included. We have normalized the different scenarios that they can fit the local PAMELA and ATIC or Fermi results well. Then the  $\gamma$ -ray emissivity by the primary sources are calculated taking their spatial distribution. The emission at a direction is calculated by integrating the emissivity of  $\gamma$ -rays along the line of sight at that direction.

### A. Contribution from Galactic pulsars

For the pulsar model we only need to consider the IC contribution to the diffuse  $\gamma$ -rays from the primary electrons/positrons. Since the pulsars are concentrated in the Galactic plane within the propagation halo, we simply calculate the total electron and positron fluxes from pulsars and the CR sources. Then we give the total IC contribution to the  $\gamma$ -rays. To some sense the pulsar scenario is similar to simply adopting a harder electron injection spectrum, as pulsar and the CR sources have similar spatial distribution.

### B. Contribution from dark matter

The  $\gamma$ -rays produced in the DM models consist of two parts: the IC radiation of the electrons/positrons when scattering with ISRF and the cosmic microwave background (CMB), and the final state radiation (FSR) emitted directly from the external legs when DM particles annihilates or decays to charged leptons. For the  $\tau^+\tau^-$  channel, the decay of tauons will produce a large number of neutral pions which can also decay into photons. This contribution is also included in the FSR.

The IC radiation is further divided into two components depending on whether the scatterings occur inside or out of the CR propagation halo. For the electrons/positrons inside the propagation halo, the ISRF is composed of the star light in optical band, the dust radiation in infrared band and the CMB. We incorporate this component in GALPROP to calculate the diffuse  $\gamma$ -ray emission (labeled as  $\phi_{\text{IC}}^{\text{in}}$ ). For the electrons/positrons out of the propagation halo only the CMB is relevant and the calculation is done separately. The equivalent spectrum of electrons/positrons out of the propagation halo can be written as

$$\frac{dn}{dE} = \frac{1}{b(E)} \int_E^\infty dE' q(\mathbf{r}, E'), \quad (8)$$

where  $q(\mathbf{r}, E)$  is the source function given in Eqs.(4) and (5) (when  $\mathbf{r}$  is located inside the propagation halo  $q(\mathbf{r}, E) = 0$ ),  $b(E) = 2.5 \times 10^{-17}(E/\text{GeV})^2 \text{ GeV s}^{-1}$  is the IC energy loss rate of the electrons/positrons when scattering off the CMB photons. Then the IC photon emissivity is simply

$$q_{\text{IC}}^{\text{out}}(\mathbf{r}, E_\gamma) = \int d\epsilon n(\epsilon) \int dE \frac{dn}{dE} \times F(\epsilon, E, E_\gamma), \quad (9)$$

where  $n(\epsilon)$  is the differential number density of CMB photon as a function of energy  $\epsilon$ . Function  $F(\epsilon, E, E_\gamma)$  is given by

$$F(\epsilon, E, E_\gamma) = \frac{3\sigma_T}{4\gamma^2\epsilon} \left[ 2q \ln q + (1 + 2q)(1 - q) + \frac{(\Gamma q)^2(1 - q)}{2(1 + \Gamma q)} \right], \quad (10)$$

with  $\sigma_T$  the Thomson cross section,  $\gamma$  the Lorentz factor of electron,  $\Gamma = 4\epsilon\gamma/m_e$ , and  $q = \frac{E_\gamma/E}{\Gamma(1-E_\gamma/E)}$ . For  $q < 1/4\gamma^2$  or  $q > 1$  we set  $F(\epsilon, E, E_\gamma) = 0$ . The flux is given through a line-of-sight integral over the emissivity

$$\phi_{\text{IC}}^{\text{out}} = \frac{1}{4\pi} \int q_{\text{IC}}^{\text{out}} dl. \quad (11)$$

The FSR is radiated in the whole DM halo. The photon yield spectrum for  $e^+e^-$  or  $\mu^+\mu^-$  channel for  $m_\chi \gg m_e, m_\mu$  can be written as [55]

$$\left. \frac{dN}{dx} \right|_i = \frac{\alpha}{\pi} \frac{1 + (1 - x)^2}{x} \log \left( \frac{s}{m_i^2} (1 - x) \right), \quad (12)$$

where  $\alpha \approx 1/137$  is the fine structure constant,  $i = e, \mu$ . For DM annihilation we have  $s = 4m_\chi^2$  and  $x = E_\gamma/m_\chi$ ; while for DM decay  $s = m_\chi^2$  and  $x = 2E_\gamma/m_\chi$  [56]. For  $\tau^+\tau^-$  channel, there is internal bremsstrahlung radiation as shown in Eq.(12) as well as the decay products from the chain  $\tau \rightarrow \pi^0 \rightarrow \gamma$ . We adopt a total parametrization as [57]

$$\left. \frac{dN}{dx} \right|_\tau = x^{-1.31} (6.94x - 4.93x^2 - 0.51x^3) e^{-4.53x}, \quad (13)$$

with the same definition of  $x$  as above.

The  $\gamma$ -ray flux along a specific direction can be written as

$$\begin{aligned} \phi_{\text{FSR}}(E_\gamma, \psi) &= C \times W(E_\gamma) \times J(\psi) \\ &= \begin{cases} \frac{\rho_\odot^2 R_\odot}{4\pi} \times \frac{\langle \sigma v \rangle}{2m_\chi^2} \frac{dN}{dE_\gamma} \times \frac{1}{\rho_\odot^2 R_\odot} \int_{\text{LOS}} \rho^2(l) dl, & \text{for annihilation} \\ \frac{\rho_\odot R_\odot}{4\pi} \times \frac{1}{m_\chi \tau} \frac{dN}{dE_\gamma} \times \frac{1}{\rho_\odot R_\odot} \int_{\text{LOS}} \rho(l) dl, & \text{for decay} \end{cases} \end{aligned} \quad (14)$$

where the integral is taken along the line-of-sight,  $W(E)$  and  $J(\psi)$  represent the particle physics factor and the astrophysical factor respectively, and  $\frac{dN}{dE_\gamma} = \frac{1}{m_\chi} \frac{dN}{dx}$ .

### C. Results

As there are discrepancies for the electron + positron spectra between ATIC and Fermi-LAT/H.E.S.S., we fit two data sets without any bias. The first one is the combination of PAMELA and ATIC data, and the second one is PAMELA + Fermi-LAT + H.E.S.S. data. The model parameters of the primary sources are accordingly different to fit the two data sets.

For PAMELA + ATIC data, the model parameters are:

- For DM annihilation,  $m_\chi = 1$  TeV, annihilation cross section<sup>2</sup>  $\langle\sigma v\rangle = 1.2 \times 10^{-23}$  cm<sup>3</sup> s<sup>-1</sup> corresponding to a boost factor  $\sim 400$  with respect to the natural value  $\langle\sigma v\rangle_0 = 3 \times 10^{-26}$  cm<sup>3</sup> s<sup>-1</sup>, and the annihilation channels are  $e^\pm$ ,  $\mu^\pm$  and  $\tau^\pm$  with equal branching ratios.
- For DM decay,  $m_\chi = 2$  TeV with life time  $\tau \sim 10^{26}$  s, and also equal branching ratios into  $e^\pm$ ,  $\mu^\pm$  and  $\tau^\pm$ .
- For pulsars, we adopt  $\alpha = 1.0$  and  $E_{\text{cut}} \sim 600$  GeV.

The choice of equal branching ratios to different lepton flavors is not only the most natural one, but also gives very good fit to the ATIC and PAMELA data. Therefore we take it as a typical configuration.

While for PAMELA + Fermi-LAT + H.E.S.S. data, the electron/positron spectra observed by Fermi-LAT and H.E.S.S. are softer and more smooth than that from ATIC, which favor a softer contribution from the extra component. For the DM models we will consider pure muon or tauon final states respectively. This is simply because both pure muon and tauon final states can fit the Fermi spectrum very well. We adopt the following model parameters:

- For DM annihilation,  $m_\chi = 1.7$  TeV, cross section  $\langle\sigma v\rangle = 1.5 \times 10^{-23}$  cm<sup>3</sup> s<sup>-1</sup> for pure  $\mu^\pm$  channel, and  $m_\chi = 3$  TeV,  $\langle\sigma v\rangle = 6.3 \times 10^{-23}$  cm<sup>3</sup> s<sup>-1</sup> for pure  $\tau^\pm$  channel.
- For DM decay,  $m_\chi = 3.4$  TeV with life time  $\tau \sim 1.45 \times 10^{26}$  s for pure  $\mu^\pm$  channel and  $m_\chi = 6$  TeV with life time  $\tau \sim 0.61 \times 10^{26}$  s for pure  $\tau^\pm$  channel.

---

<sup>2</sup> Note that the cross section is 2 times smaller than the one derived in Ref. [28]. This is because the DM substructures contribute a boost factor  $\sim 2$  to the local electrons/positrons.

- For pulsars,  $\alpha = 1.4$  and  $E_{\text{cut}} \sim 800$  GeV.

The spectra of the diffuse  $\gamma$ -rays of these models for the six different sky regions are shown in Figs. 4 and 5. The observational data from EGRET [3] are shown for comparison. For region D, we also plot the preliminary results from Fermi-LAT [31]. In Fig. 4 the DM model to fit the PAMELA + Fermi-LAT + H.E.S.S. data is pure  $\mu^\pm$  channel, while in Fig. 5 it is pure  $\tau^\pm$  channel.

We first look at the IC component from the primary sources, which is large at the energy range  $\lesssim 10$  GeV. We find that the current EGRET data can already constrain or exclude some of the model configurations. The IC contribution from the primary sources is more significant in the high latitude regions (e.g., E and F) where the Galactic background is lower. From panel F of Fig. 4 we can see that the annihilation DM model which fits the PAMELA + ATIC data will produce  $\sim 2$  times larger  $\gamma$ -ray fluxes than the EGRET data. For parameters fitting to PAMELA + Fermi-LAT + H.E.S.S. data with  $\mu^\pm$  channel this excess is not so remarkable. While for  $\tau^\pm$  channel this excess is very clear as shown in panels E and F in Fig. 5. This may indicate that, 1) the annihilation DM model which fits to PAMELA + ATIC data with equal flavor final states, or to PAMELA + Fermi-LAT + H.E.S.S. data with  $\tau^\pm$  final state, is excluded; or 2) the minimum mass of the DM substructures  $M_{\text{min}}$  is larger than  $10^{-6} M_\odot$ . However, the constraints on the decaying DM model is much weaker. The IC contribution from pulsar electrons/positrons is always negligible.

Secondly we notice an important feature of the diffuse  $\gamma$ -ray spectra from the FSR component of DM models. From Figs. 4 and 5 we can find that for the DM model, there is always a bump at energies about several hundred GeV to TeV due to the FSR. This spectral feature is more remarkable in high latitude sky regions. For the annihilation DM case this bump structure is larger than the case of decay. Because the large amount of  $\gamma$ -rays production, this high energy bump is extremely clear for tauon final states as can be seen in Fig. 5.

In order to see the detectability of this smoking gun signature of DM models at Fermi-LAT, we plot the expected errorbars at the figures, including the systematic ones from Ref. [31] and the statistical ones calculated using the effective area and acceptance given in Ref. [58], for 1-yr exposure of Fermi-LAT telescope. We have assumed the central value of the spectra is as the background contribution. It is shown that Fermi-LAT will have the

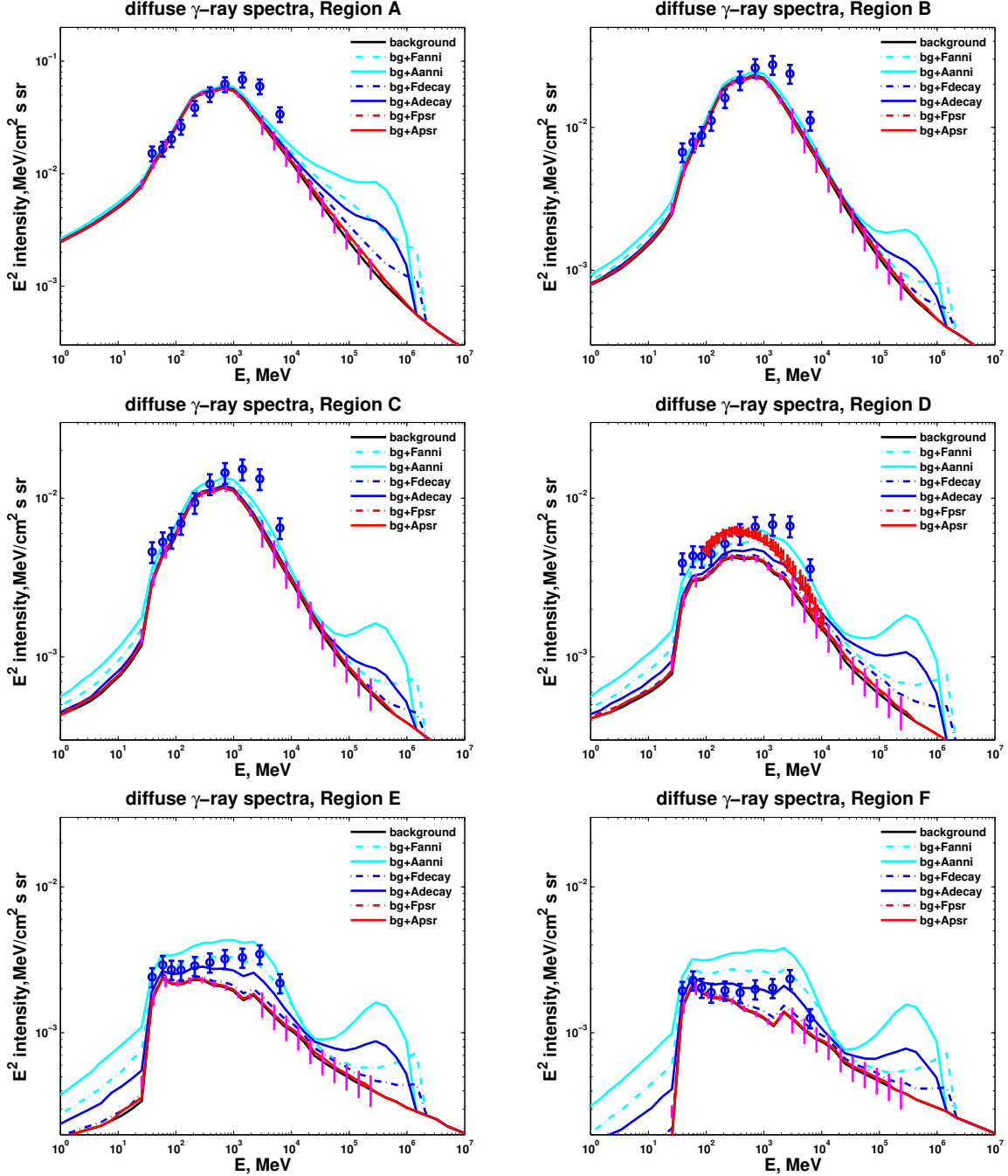


FIG. 4: The diffuse  $\gamma$ -ray spectra for six sky regions. In this plot, the final state of DM models fit to PAMELA + Fermi-LAT + H.E.S.S. data is pure  $\mu^\pm$ . The black-solid line denotes the background. The captions of other lines, for example “bg+Fanni”, mean that background plus DM **annihilation** contribution with fit to the **F**ermi-LAT electrons. Also plotted are EGRET data (blue circles with error bars, [3]), preliminary Fermi-LAT mid-latitude diffuse  $\gamma$ -ray emission (red triangles with error bars, [31]) and the expected performance of Fermi-LAT with 1-yr exposure (magenta bars).

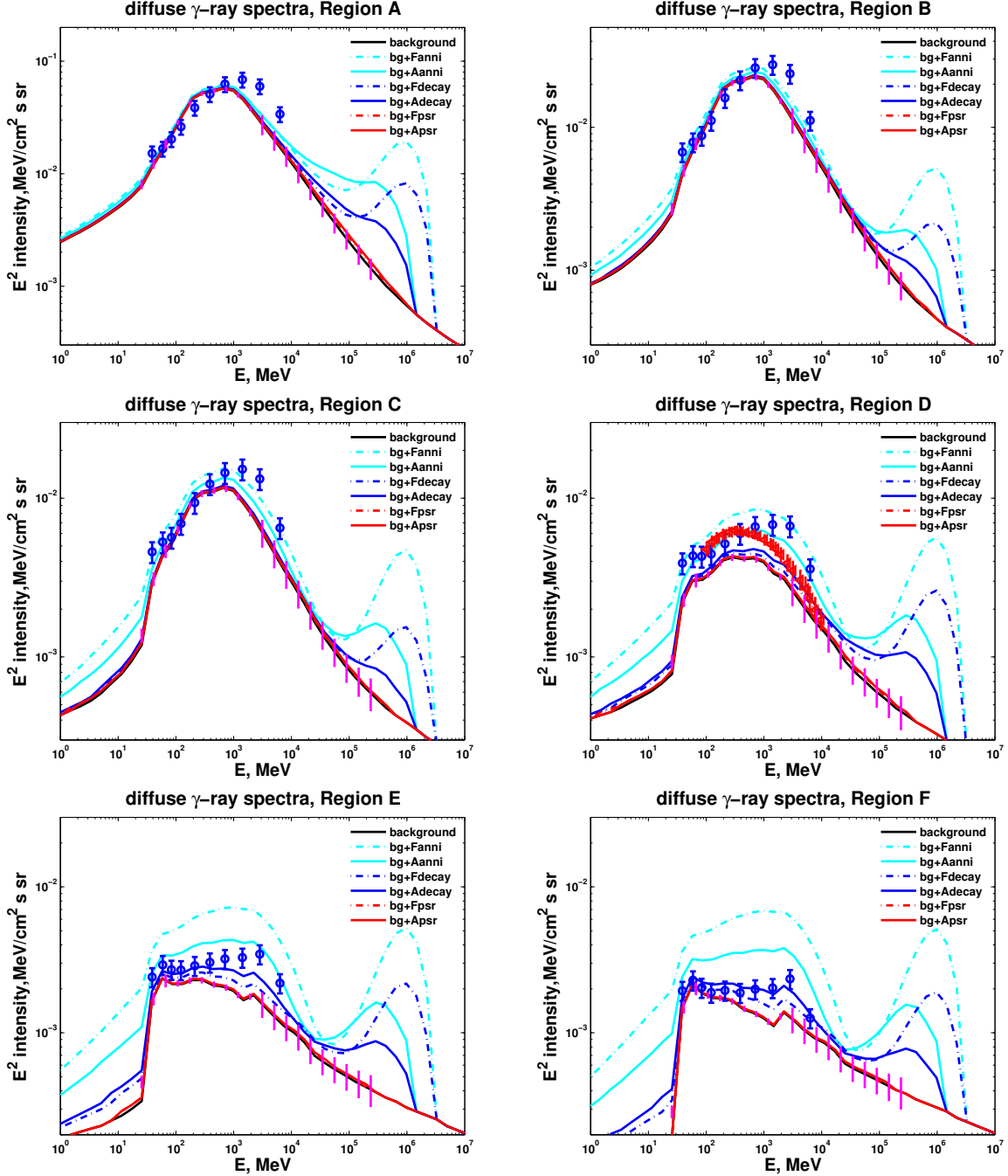


FIG. 5: Same as Fig. 4 except that the DM models fit to PAMELA + Fermi-LAT + H.E.S.S. data are with  $\tau^\pm$  final states.

potential to measure the all-sky  $\gamma$ -ray spectra precisely up to  $\sim 300$  GeV. It will be very interesting if Fermi-LAT can observe some spectral distortion of the diffuse  $\gamma$ -ray spectra, such as a dip or an “ankle-like” structure.

Due to our estimate of the Fermi-LAT errors after 1-yr exposure we find the pulsar

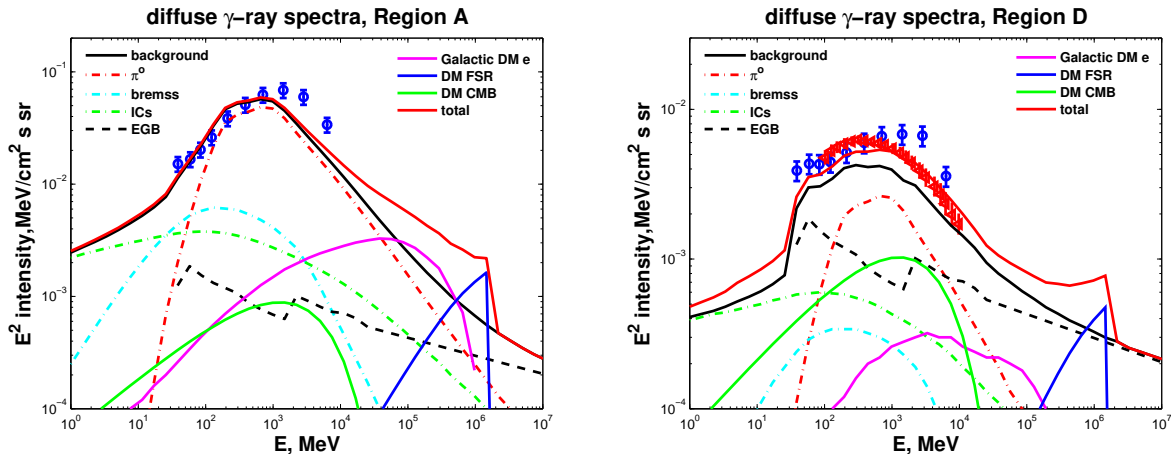


FIG. 6: Contributions of each component for the annihilation DM model with  $\mu^\pm$  final states, which is to fit the PAMELA + Fermi-LAT + H.E.S.S. data. Black solid line: total background with  $\pi^0$  component (red dot-dashed), IC (green dot-dashed), bremsstrahlung (cyan dot-dashed) and the isotropic extragalactic background (black dashed); magenta solid line: IC of DM electrons inside the diffusion halo; blue solid line: FSR from DM; green solid line: IC of DM electrons outside the diffusion halo. The sum of these components are represented in red solid line.

scenario does not change the diffuse  $\gamma$ -ray spectra of the conventional background. While for DM scenarios the signatures on the  $\gamma$ -ray spectra may be clear enough to be detected by Fermi-LAT after 1-yr observation, only except the case normalized to PAMELA + Fermi-LAT + H.E.S.S. data with muon final states. In that case the changes on the  $\gamma$ -ray spectra for energies less than several hundred GeV are not very significant and we may need the measurement up to about 1 TeV with very high precision to explore this model.

To better illustrate the contributions of each component, we plot the detailed results in Figs. 6 and 7 for regions A and D respectively, taking the  $\mu^\pm$  and  $\tau^\pm$  final states for annihilation DM model as examples. From these figures we clearly see that the FSR from the DM scenario shows distinctive feature at the spectra. If these features are detected, the DM scenario will be strongly favored.

## V. CONCLUSION AND DISCUSSION

In this work we recalculate the all-sky diffuse  $\gamma$ -ray emission taking the recent CR  $e^\pm$  excesses into account. We consider three typical models: Galactic pulsars, DM annihilation

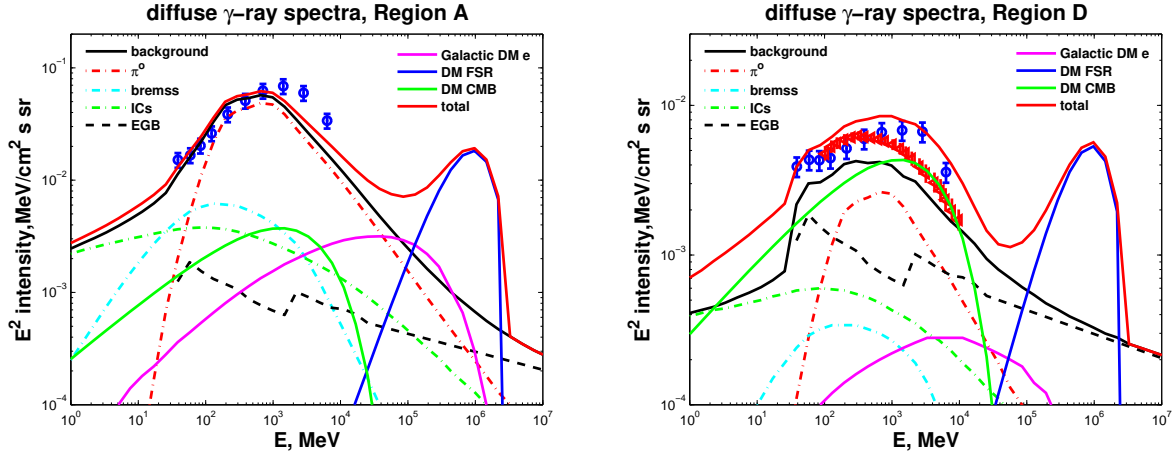


FIG. 7: Same as Fig. 6, but for  $\tau^\pm$  final states of DM annihilation.

and DM decay. For each model, we adopt typical parameter settings which can recover the electron/positron observations. We then investigate the diffuse  $\gamma$ -ray emissions, generated through IC scattering of the electrons/positrons off the ISRF and/or CMB and the FSR from DM annihilation or decay. For the DM annihilation model, the substructure effect is included according to the newest high resolution N-body simulation.

Our results show that, the contribution to diffuse  $\gamma$ -rays from pulsars is always negligible in any region of the sky. While for DM models, there are some interesting features which deserve our attention. We find that the emission at high Galactic latitudes is actually better than that from the Galactic plane in discriminating different models due to the low background in the former case. In addition, the emission region excluding the GC will also be less dependent on the DM spatial profile, which is shown to be the major uncertainty source of the  $\gamma$ -ray emission [28]. We find the DM annihilation models always over-produce  $\gamma$ -rays in high latitude regions (E and F in Figs. 4 and 5) exceeding the EGRET data. Taking into account the uncertainties of the background and observations, the DM annihilation model with  $\mu^\pm$  final states to fit the PAMELA + Fermi-LAT + H.E.S.S. data can marginally survive under the EGRET observations. For the DM decay model, the IC contribution is less significant and the EGRET data are well explained.

Furthermore, there is always a remarkable bump at the  $\gamma$ -ray spectra at energies about several hundred GeV to TeV in DM models due to the FSR component. Together with the background contribution, the total diffuse  $\gamma$ -ray emission will show a flattening or even arising behavior in the  $E^2 dN/dE$  plot. Even if for DM decay model, this flattening or arising

is able to be observed, especially for the models with  $\tau^\pm$  final states and normalization to PAMELA + ATIC data. This bump feature is also more remarkable at high latitudes. We expect that the forthcoming Fermi diffuse  $\gamma$ -ray data will be a powerful tool in distinguishing different origins of the CR electrons/positrons excesses.

If the future Fermi data show that the diffuse  $\gamma$ -ray spectra follow the conventional background the astrophysical origins of the cosmic  $e^\pm$  excesses will be strongly favored. In such a case only a small window is opened for the DM scenario. In order to further constrain the DM scenario we have to detect the  $\gamma$ -ray spectra up to higher energies.

### Acknowledgments

We thank I. V. Moskalenko for helpful discussion during the *1st workshop on gamma ray astronomy at high altitude* at Hebei, China. This work is supported in part by the Natural Sciences Foundation of China (No. 10773011) and by the Chinese Academy of Sciences under the grant No. KJCX3-SYW-N2.

- 
- [1] A. W. Strong and I. V. Moskalenko, *Astrophys. J.* **509**, 212 (1998). [arXiv:astro-ph/9807150].
  - [2] I. V. Moskalenko and A. W. Strong, *Astrophys. J.* **493**, 694 (1998). [arXiv:astro-ph/9710124].
  - [3] S. D. Hunter *et. al.*, *Astrophys. J.* **481**, 205 (1997).
  - [4] F. W. Stecker, S. D. Hunter and D. A. Kniffen, *Astropart. Phys.* **29**, 25 (2008) [arXiv:0705.4311 [astro-ph]].
  - [5] P. Gralewicz, J. Wdowczyk, A. W. Wolfendale, L. Zhang, *Astron. & Astrophysics* **318**, 925 (1997);  
M. Mori, *Astrophys. J.* **478**, 225 (1997);  
T. A. Porter, R. J. Protheroe, *J. Phys. G* **23**, 1765 (1997);  
M. Pohl, J. A. Esposito, *Astrophys. J.* **507**, 327 (1998);  
F. A. Aharonian, A. M. Atoyan, *Astron. & Astrophysics* **362**, 937 (2000).
  - [6] A. W. Strong, I. V. Moskalenko, O. Reimer, *Astrophys. J.* **537**, 763 (2000).
  - [7] A. W. Strong, I. V. Moskalenko and O. Reimer, *Astrophys. J.* **613**, 962 (2004) [arXiv:astro-ph/0406254].

- [8] W. de Boer, *New Astron. Rev.* **49**, 213 (2005) [arXiv:hep-ph/0408166].
- [9] W. de Boer, C. Sander, V. Zhukov, A. V. Gladyshev and D. I. Kazakov, *Astron. Astrophys.* **444**, 51 (2005) [arXiv:astro-ph/0508617].
- [10] X. J. Bi, J. Zhang, Q. Yuan, J. L. Zhang and H. Zhao, *Phys. Lett. B* **668**, 87 (2008) [arXiv:astro-ph/0611783].
- [11] X. J. Bi, J. Zhang, and Q. Yuan, *Phys. Rev. D* **78**, 043001 (2008) [arXiv:0712.4038 [astro-ph]].
- [12] O. Adriani *et al.*, *Nature* **458**, 607 (2009) [arXiv:0810.4995 [astro-ph]].
- [13] J. Chang *et al.*, *Nature* **456** (2008) 362.
- [14] S. Torii *et al.*, arXiv:0809.0760 [astro-ph].
- [15] F. Aharonian *et al.*, *Phys. Rev. Lett.* **101**, 261104 (2008) [arXiv:0811.3894 [astro-ph]].
- [16] F. Aharonian *et al.*, arXiv:0905.0105 [astro-ph.HE].
- [17] A. A. Abdo *et al.*, *Phys. Rev. Lett.* **102**, 181101 (2009) [arXiv:0905.0025 [astro-ph.HE]].
- [18] D. Hooper, P. Blasi and P. D. Serpico, *JCAP* **0901**, 025 (2009) [arXiv:0810.1527 [astro-ph]].
- [19] H. Yuksel, M. D. Kistler and T. Stanev, arXiv:0810.2784 [astro-ph].
- [20] S. Profumo, arXiv:0812.4457 [astro-ph].
- [21] H. B. Hu, Q. Yuan, B. Wang, C. Fan, J. L. Zhang and X. J. Bi, *Astrophys. J.* **700**, L170 (2009) [arXiv:0901.1520 [astro-ph]].
- [22] Y. Fujita, K. Kohri, R. Yamazaki and K. Ioka, arXiv:0903.5298 [astro-ph.HE].
- [23] L. Bergstrom, T. Bringmann and J. Edsjo, *Phys. Rev. D* **78**, 103520 (2008) [arXiv:0808.3725 [astro-ph]].
- [24] V. Barger, W. Y. Keung, D. Marfatia and G. Shaughnessy, *Phys. Lett. B* **672**, 141 (2009) [arXiv:0809.0162 [hep-ph]].
- [25] M. Cirelli, M. Kadastik, M. Raidal and A. Strumia, *Nucl. Phys. B* **813**, 1 (2009) [arXiv:0809.2409 [hep-ph]].
- [26] P. F. Yin, Q. Yuan, J. Liu, J. Zhang, X. J. Bi, S. H. Zhu, and X. M. Zhang, *Phys. Rev. D* **79**, 023512 (2009) [arXiv:0811.0176 [hep-ph]].
- [27] G. Bertone, M. Cirelli, A. Strumia and M. Taoso, *JCAP* **0903**, 009 (2009) [arXiv:0811.3744 [astro-ph]].
- [28] J. Zhang, X. J. Bi, J. Liu, S. M. Liu, P. F. Yin, Q. Yuan and S. H. Zhu, *Phys. Rev. D* **80**, 023007 (2009) [arXiv:0812.0522 [astro-ph]].
- [29] L. Bergstrom, G. Bertone, T. Bringmann, J. Edsjo and M. Taoso, *Phys. Rev. D* **79**, 081303

- (2009) [arXiv:0812.3895 [astro-ph]].
- [30] E. Borriello, A. Cuoco and G. Miele, *Astrophys. J.* **699**, L59 (2009) [arXiv:0903.1852 [astro-ph.GA]].
- [31] T. A. Porter, arXiv:0907.0294 [astro-ph.HE].
- [32] V. Barger, Y. Gao, W. Y. Keung, D. Marfatia and G. Shaughnessy, *Phys. Lett. B* **678**, 283 (2009) [arXiv:0904.2001 [hep-ph]].
- [33] M. Cirelli and P. Panci, arXiv:0904.3830 [astro-ph.CO].
- [34] I. Cholis, G. Dobler, D. P. Finkbeiner, L. Goodenough, T. R. Slatyer and N. Weiner, arXiv:0907.3953 [astro-ph.HE].
- [35] V. Springel *et al.*, *Nature* **456**, 73 (2008).
- [36] A. W. Strong, I. V. Moskalenko and O. Reimer, *Astrophys. J.* **613**, 956 (2004) [arXiv:astro-ph/0405441].
- [37] T. Delahaye, F. Donato, N. Fornengo, J. Lavallo, R. Lineros, P. Salati and R. Taillet, *Astron. Astrophys.* **501**, 821 (2009) arXiv:0809.5268 [astro-ph].
- [38] D. Grasso *et al.* [FERMI-LAT Collaboration], arXiv:0905.0636 [astro-ph.HE].
- [39] O. Adriani *et al.*, *Phys. Rev. Lett.* **102**, 051101 (2009) [arXiv:0810.4994 [astro-ph]].
- [40] D. A. Frail, M. F. Bietenholz, C. B. Markwardt, and H. Oegelman, *Astrophys. J.* **475**, 224 (1997)
- [41] G. G. Pavlov, O. Y. Kargaltsev, D. Sanwal, and G. P. Garmire, *Astrophys. J.* **554**, 189 (2001)
- [42] F. J. Lu, Q. D. Wang, B. Aschenbach, P. Durouchoux and L. M. Song, *Astrophys. J.* **568**, L49 (2002)
- [43] F. Aharonian *et al.* [H.E.S.S. Collaboration], *Astron. Astrophys.* **448**, L43 (2006) [arXiv:astro-ph/0601575].
- [44] X. H. Li, F. J. Lu and Z. Li, *Astrophys. J.* **682**, 1166 (2008) [arXiv:0707.4279v2 [astro-ph]].
- [45] L. Zhang and K. S. Cheng, *Astron. Astrophys.* **368**, 1063 (2001)
- [46] G. Jungman, M. Kamionkowski and K. Griest, *Phys. Rept.* **267**, 195 (1996). [arXiv:hep-ph/9506380].
- [47] G. Bertone, D. Hooper and J. Silk, *Phys. Rept.* **405**, 279 (2005) [arXiv:hep-ph/0404175].
- [48] T. Sjostrand, S. Mrenna and P. Skands, *JHEP* **0605**, 026 (2006) [arXiv:hep-ph/0603175].
- [49] J. Einasto, *Trudy Inst. Astrofiz. Alma-Ata* **51**, 87 (1965)
- [50] D. P. Finkbeiner, *Astrophys. J.* **614**, 186 (2004) [arXiv:astro-ph/0311547].

- [51] A. Pinzke, C. Pfrommer and L. Bergstrom, arXiv:0905.1948 [astro-ph.HE].
- [52] S. Hofmann, D. J. Schwarz and H. Stoecker, Phys. Rev. D **64**, 083507 (2001).
- [53] X. L. Chen, M. Kamionkowski and X. M. Zhang, Phys. Rev. D **64**, 021302 (2001).
- [54] V. Springel *et al.*, arXiv:0809.0898 [astro-ph].
- [55] L. Bergstrom, T. Bringmann, M. Eriksson and M. Gustafsson, Phys. Rev. Lett. **94**, 131301 (2005) [arXiv:astro-ph/0410359].
- [56] R. Essig, N. Sehgal and L. E. Strigari, arXiv:0902.4750 [hep-ph].
- [57] N. Fornengo, L. Pieri and S. Scopel, Phys. Rev. D **70**, 103529 (2004) [arXiv:hep-ph/0407342].
- [58] W. B. Atwood *et al.* [LAT Collaboration], Astrophys. J. **697**, 1071 (2009) [arXiv:0902.1089 [astro-ph.IM]].
- [59] J. H. Chapell and W. R. Webber, Proc. 17th Int. Cosmic Ray Conf. (Paris), **2**, 59 (1981).
- [60] R. C. Maehl, J. F. Ormes, A. J. Fisher, and F. A. Hagen, Astrophys. Space Sci., **47**, 163 (1977).
- [61] A. Lukasiak, F. B. McDonald and W. R. Webber, in *Proceedings of the 26th International Cosmic Ray Conference* (AIP, Salt Lake City, 1999), Vol. 3, p. 41.
- [62] J. J. Engelmann, P. Ferrando, A. Soutoul, P. Goret and E. Juliusson, Astron. Astrophys. **233**, 96 (1990).
- [63] M. A. Du Vernois, J. A. Simpson and M. R. Thayer, Astron. Astrophys. **316**, 555 (1996).
- [64] R. Dwyer, Astrophys. J. **224**, 691 (1978).
- [65] A. J. Davis *et al.*, in *Acceleration and Transport of Energetic Particles Observed in the Heliosphere*, edited by R. A. Mewaldt *et al.*, AIP Conf. Proc. **528** (AIP, New York, 2000), p. 421.
- [66] J. J. Connell, Astrophys. J. **501**, L59 (1998).
- [67] W. R. Binns *et al.*, in *Proceedings of the 26th International Cosmic Ray Conference* (AIP, Salt Lake City, 1999), Vol. 3, p. 21.
- [68] T. Sanuki *et al.*, Astrophys. J. **545**, 1135 (2000). [arXiv:astro-ph/0002481].
- [69] J. Alcaraz *et al.* [AMS Collaboration], Phys. Lett. B **490**, 27 (2000).
- [70] M. Boezio *et al.*, Astrophys. J. **532**, 653 (2000).
- [71] S. W. Barwick *et al.*, Astrophys. J. **498**, 779 (1998).
- [72] S. W. Barwick *et al.* [HEAT Collaboration], Astrophys. J. **482**, L191 (1997). [arXiv:astro-ph/9703192].

- [73] S. Coutu *et al.*, in *Proceedings of the 27th International Cosmic Ray Conference* (Hamburg, 2001), Vol. 5, p. 1687.